Tailoring of Phononic Band Structures in Colloidal Crystals

J. Baumgartl,* M. Zvyagolskaya, and C. Bechinger
Physikalisches Institut, Universität Stuttgart, 70550 Stuttgart, Germany
(Received 2 August 2007; published 14 November 2007)

We report an experimental study of the elastic properties of a two-dimensional (2D) colloidal crystal subjected to light-induced substrate potentials. In agreement with recent theoretical predictions [H. H. von Grünberg and J. Baumgartl, Phys. Rev. E **75**, 051406 (2007).] the phonon band structure of such systems can be tuned depending on the symmetry and depth of the substrate potential. Calculations with binary crystals suggest that phononic band engineering can be also performed by variations of the pair potential and thus opens novel perspectives for the fabrication of phononic crystals with band gaps tunable by external fields.

DOI: 10.1103/PhysRevLett.99.205503 PACS numbers: 63.20.Dj, 63.22.+m, 82.70.Dd

Materials with periodic variations in their elastic properties have currently received much interest as phononic crystals. Analogue to light propagation in photonic crystals [1,2], the transmitted spectrum of sound waves traveling through phononic crystals exhibit band gaps whose frequency is determined by the length scale on which the elastic properties are modulated. Fabrication of phononic crystals is achieved by embedding regular arrays of elastic inclusions in an appropriate matrix. Experiments with millimeter-sized inclusions [3,4] or sub-micron-sized holes immersed in elastic host materials [5,6] indeed show acoustic band gaps at ultrasonic, sonic, and hypersonic frequencies. Recent Brillouin spectroscopy measurements on crystals made of sub-micron-sized colloidal particles immersed in a liquid matrix demonstrated band gaps in the hypersonic regime with the possibility of tuning the band gap by exchange of the surrounding liquid [7].

In this Letter, we experimentally investigate the phononic properties of a two-dimensional (2D) crystal of colloidal particles being subjected to a periodic substrate potential. Depending on the substrate strength and particle interactions, the phononic band structure and thus the position and width of phononic band gaps can be largely tuned. Because this concept applies not only to micron-sized colloids but also to much smaller particles, this suggests tailoring the phononic properties of atoms or molecules confined to extended optical lattices [8].

Experiments were performed with an aqueous suspension of highly charged polystyrene spheres with diameter $\sigma = 2.4\ \mu$m and a polydispersity below 4%. The particles interact via a screened Coulomb potential $\Phi(r) \propto Z^2 \exp(-\kappa r)/r$ with $Z \approx 10\,000$ the renormalized surface charge and $\kappa^{-1} \approx 300$ nm the screening length. Both values were determined according to a procedure described in [9]. As the sample cell we used a cuvette made of fused silica with 200 μm spacing between the top and bottom plate which was connected to a standard closed deionization circuit to maintain stable ionic conditions during the measurements [10]. After sedimentation, the particles form a 2D colloidal system close to the bottom plate.

One- and two-dimensional substrate potentials were created by superimposing two perpendicularly aligned one-dimensional periodic interference patterns created with a $P = 5W$ frequency-doubled Nd:YVO_4 laser (wavelength = 532 nm). The polarizations of the interference patterns were adjusted perpendicularly, therefore they act as two independent 1D periodic substrate potentials for the colloidal particles $U_i(x) = U_0^i \cos(2\pi x/d_i)$ with U_0^i the potential amplitude, d_i the lattice constant and $i = 1, 2$ [11]. Because the potential amplitude U_0^i scales linearly with the intensities of the laser beams [12] this allows the continual adjustmentof the strength of the underlying laser potentials. An additional laser beam was scanned around the central region of the sample to create a boundary box whose size could be continuously adjusted by a pair of computer-controlled galvanostatically driven mirrors. This allowed us to adjust the particle density ρ with an accuracy of $\Delta\rho/\rho \approx 0.01$ [13].

First, we continuously decreased the mean particle distance $a = \sqrt{2/\sqrt{3}\rho}$ to approximately 4 μm where under our salt conditions spontaneous crystallization of the colloidal monolayer occurs. Next, the lattice constants d_1 and d_2 were chosen to meet commensurate conditions, i.e., $d_1 = (\sqrt{3}/2)a \approx 3.5\ \mu$m and $d_2 = a/2 \approx 2\ \mu$m (see Fig. 1). Particle positions were determined for different combinations of interference pattern intensities $\{U_0^1, U_0^2\}$ from sequences consisting of several thousand images using digital video microscopy at an acquisition rate of 2 frames per second [9]. From these data we finally obtained the particle trajectories $\vec{r}_\mu(t) = [x_\mu(t), y_\mu(t)]$ with $\mu = 1, \ldots, N$ and t the time. To avoid boundary effects, we only considered the central region of the field of view (300 μm $\times$ 200 μm) containing $N \approx 1000$ particles.

For the experimental determination of the phononic band structure we followed the approach already introduced in [14–16], which is based on the analysis of the dynamical matrix. Briefly, the branch $\lambda_s(\vec{q})$ of the phononic band structure with $\vec{q}$ the wave vector and polarization s is given by the eigenvalue of the dynamical matrix

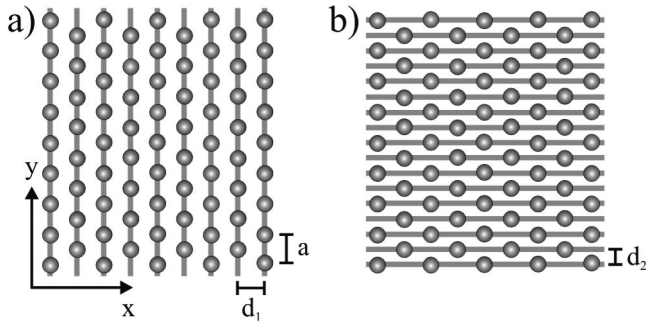

FIG. 1. Illustration of the colloidal system subjected to commensurate optical interference patterns. Gray dots represent colloidal particles and gray lines indicate the minima of the light-induced 1D periodic potentials. The lattice constants d_1 and d_2 of the 1D periodic potentials are chosen to be commensurate with the mean particle distance a.

denoted as $D_{\alpha\beta}(\vec{q})$ (α, $\beta = x$, y). The latter is obtained from the measured particle displacements $\vec{u}(\vec{R}, t)$ relative to their lattice sites $\vec{R}$

$$D_{\alpha\beta}(\vec{q}) = k_B T / \langle u^*_\alpha(\vec{q}, t) u_\beta(\vec{q}, t) \rangle_t, \tag{1}$$

with $\vec{u}(\vec{q}, t)$ the Fourier transform of $\vec{u}(\vec{R}, t)$ and $\langle \ldots \rangle_t$ the temporal average. Using the equipartition theorem, this expression has been derived within the harmonic approximation of the potential energy

$$H = 1/2 \sum_{\vec{q},\alpha,\beta} u^*_\alpha(\vec{q}) D_{\alpha\beta}(\vec{q}) u_\beta(\vec{q}), \tag{2}$$

which has been experimentally confirmed to be valid for colloidal systems [15]. Note, that due to the absence of true long-range order in 2D systems, the lattice sites $\vec{R}$ have to be determined through temporal averaging [17,18]. Within the harmonic approximation the pair interaction between particles can be modeled as springs with the spring constant k_0 given by the second derivative of the pair potential at the mean particle distance $k_0 = [d^2\Phi(r)/dr^2]_{r=a}$. With the corresponding values Z and κ taken from above we obtain $k_0 \approx 150 k_B T/\sigma^2 \approx 1 \times 10^{-7}$ J/m^2. The periodic substrates U_0^i introduce an additional set of springs which pin the particles to their lattice sites $\vec{R}$ with spring constants $k_i = U_0^i (2\pi/d_i)^2$. With the laser intensities used in our experiments we achieved maximum values of $k_i \approx 2.5 k_0$. Since the phononic band structure depends only on the ratio between pair and particle-substrate interaction, in the following it will be expressed in units of k_0. We confirmed the harmonic approximation to be valid over the entire range of observed displacements ($|u_\alpha| \leq 1$ μm) by determining the effective single-particle potential $U_{\text{eff}}(u_\alpha)/k_B T = -\ln[P(u_\alpha)]$ with $P(u_\alpha)$ the normalized particle-displacement distribution.

We will start our discussion by first describing the results obtained when only a single 1D substrate potential was applied ($U_0^2 = 0$) (see Fig. 2). A typical snapshot of the colloidal crystal is shown in Fig. 2(a) (the 1D laser potential which is aligned vertically is invisible because it is blocked with optical filters). Figure 2(b) illustrates the irreducible path along which the phonon band structure has been analyzed. It corresponds to that route which circumvents that part of the first Brillouin zone (gray area) being the smallest repeat unit of the band structure. Due to the two-fold symmetry of the 1D periodic substrate potential, this unit comprises a quarter of the first Brillouin zone. Figures 2(c)–2(h) show the 2D pair correlation function $g(x, y)$ and the corresponding phonon band structure for increasing laser intensities $k_1/k_0 = 0$ (spontaneous crystal) (c),(f), $k_1/k_0 = 1$ (d),(g) and $k_1/k_0 = 2.5$ (e),(h), respectively. Since the particles' motion becomes more confined in the direction perpendicular to the potential troughs, the fluctuations in x and y direction become

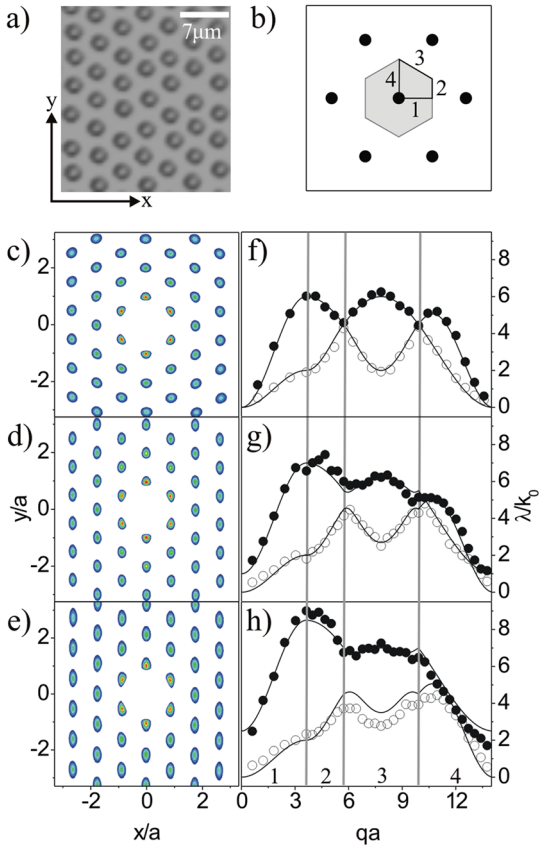

FIG. 2 (color online). Experimental realization of a 2D colloidal crystal on a 1D periodic substrate [see Fig. 1(a)]. (a) Micrograph of the 2D colloidal crystal in the central region of the field of view (300 μm $\times$ 200 μm). (b) Zero and first order Bragg peaks (black dots) and first Brillouin zone (gray area). The black solid line represents the irreducible path along which the phonon band structure is plotted and the path sections are marked by numbers. (c)–(e) 2D correlation function $g(x, y)$ and (f)–(h) phonon band structure $\lambda_s(q)$ along the irreducible path for (c),(f) the spontaneous crystal, i.e., $k_1/k_0 = 0$, (d),(g) $k_1/k_0 = 1$, and (e),(h) $k_1/k_0 = 2.5$. Closed and open symbols refer to the upper and lower band, respectively. Solid lines represent band structures calculated in the framework of harmonic lattice dynamics [14].

asymmetric with increasing (k_1/k_0) as this is observed in the corresponding $g(x, y)$-plots.

From the above it is clear that changes in $g(x, y)$ also affect the dynamical matrix and thus the phononic band structure. As we will demonstrate in the following, those changes strongly depend on the polarization of the phonons. Usually, the polarization s refers to longitudinal and transversal modes in the direction of high crystal symmetry. Because we also determined the band structure in directions with lower symmetry, in the following we will refer to the different polarizations by their vertical position in Figs. 2(f)–2(h) as lower $(s = l)$ and upper $(s = u)$ bands instead. Interestingly, both bands are affected by the substrate potential in a rather different way. We observe a pure shift of the upper band $\lambda_u(\vec{q})$ (closed symbols) along the sections 1 and 2 while the lower band $\lambda_l(\vec{q})$ (open symbols) is not affected. This can be easily understood because $\lambda_u(\vec{q})$ and $\lambda_l(\vec{q})$ have polarization vectors in the x and the y direction along these sections, respectively. As a consequence, $\lambda_u(\vec{q})$ is increased by the spring constant k_1/k_0 of the periodic potential. The bands have the same polarization along section 4 of the irreducible path. Therefore, the upper band is not influenced by the periodic potential and the lower band is shifted by k_1/k_0. We observe a different behavior along section 3; here, both the upper and the lower band are influenced because the respective polarization does not point in the x- and the y-direction. The upper band becomes largely deformed and is almost entirely flattened in Fig. 2(h). Because the group velocity $\vec{v}(\vec{q}) \propto \nabla\sqrt{\lambda(\vec{q})}$ vanishes in those regions, this opens interesting perspectives regarding the tailoring of acoustic and thermal properties of 2D crystals. We also compared the experimentally determined band structures with calculations based on the harmonic approximation [14] using k_1/k_0 as a fit parameter, the latter being in excellent agreement with the corresponding values independently obtained from κ^{-1} and U_0^1. The calculated band structures are plotted as solid lines in Figs. 2(f)–2(h).

Similar experiments have been also performed for 2D substrate potentials $(\{U_0^1, U_0^2\} \neq \{0, 0\})$ and demonstrate that both the upper and the lower band can be individually shifted and deformed by the presence of the substrate potentials. Rather than showing a specific path through the Brillouin zone, here we have chosen a 2D representation of the phononic band structure which is shown in Fig. 3 for different combinations of substrate strengths. For comparison, we also show calculated 2D phonon band structures obtained within the harmonic approximation using k_1/k_0 and k_2/k_0 as fit parameters [14]. For the substrate-free case where $\{k_1/k_0, k_2/k_0\} = \{0, 0\}$, as expected we observe the sixfold symmetry of a spontaneous crystal [Fig. 3(a)]. In Fig. 3(b), the spring constants are $\{k_1/k_0, k_2/k_0\} = \{1.4, 0.2\}$. Here, the symmetry breaks down to a two-fold symmetry due to the dominating k_1. Figure 3(c) corresponds to the situation where both interference patterns have identical strengths $\{k_1/k_0, k_2/k_0\} = \{1.5, 1.5\}$ and as a consequence the sixfold symmetry is restored. Finally, Fig. 3(d) shows the case where $\{k_1/k_0, k_2/k_0\} = \{0.5, 1.5\}$. Similarly to Fig. 3(b) we find a twofold symmetry but here rotated by 90° because of $k_2/k_0 > k_1/k_0$.

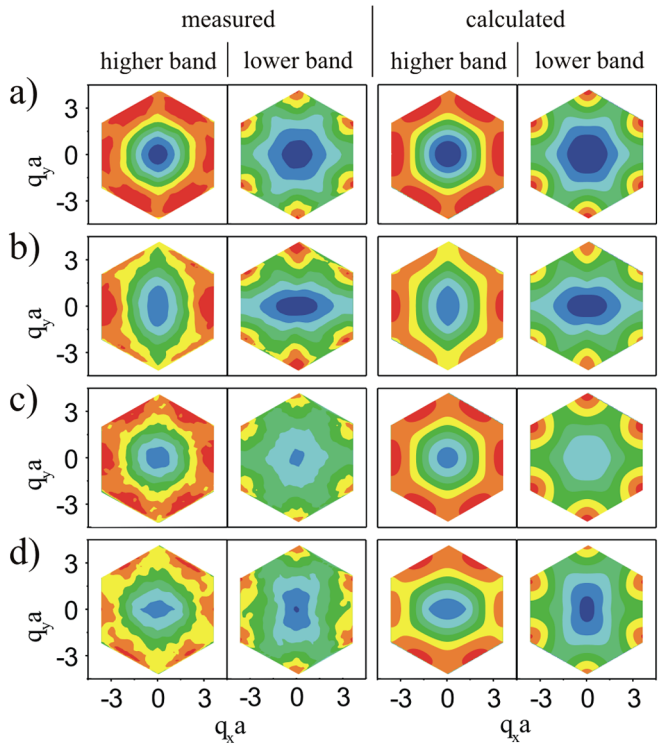

FIG. 3 (color online). Experimental realization of a 2D colloidal crystal in the presence of two 1D periodic substrates rotated by 90° (see Fig. 1). The graphs are 2D contour plots of the phonon band structure in the first Brillouin zone derived from experimental (left column) and analytical data (right column). (a) $\{k_1/k_0, k_2/k_0\} = \{0, 0\}$. (b) $\{k_1/k_0, k_2/k_0\} = \{1.4, 0.2\}$. (c) $\{k_1/k_0, k_2/k_0\} = \{1.5, 1.5\}$. (d) $\{k_1/k_0, k_2/k_0\} = \{0.5, 1.5\}$. Experimental contour plots were determined for approximately 800 $\vec{q}$-values. Calculated plots were obtained in the framwork of harmonic lattice dynamics using approximately 3000 $\vec{q}$-values [14].

After having discussed the possibility to tailor phononic band structures by subjecting monolayers to substrate potentials, finally, we want to discuss whether phononic band engineering can also be achieved by adjustable anisotropic pair potentials. Here, we exemplarily consider a system with magnetic dipole-dipole interactions $\Phi_m(\vec{r}) = \vec{d}^2/|\vec{r}|^3 - 3(\vec{d}\cdot\vec{r})^2/|\vec{r}|^5$. For paramagnetic particles the dipole moment $\vec{d}$ scales as $\vec{d} = \chi\vec{B}$ with χ the magnetic susceptibility and $\vec{B}$ the magnetic field. The pair interaction becomes anisotropic when the magnetic field is not applied perpendicular to the plane of the 2D crystal. Our calculations based on the approach in [14] indeed show that tuning of phononic bands is possible under such conditions, however, we also find that anisotropic pair potentials are not sufficient to create band gaps in monodisperse systems. This is because only acoustic branches exist in such sys-

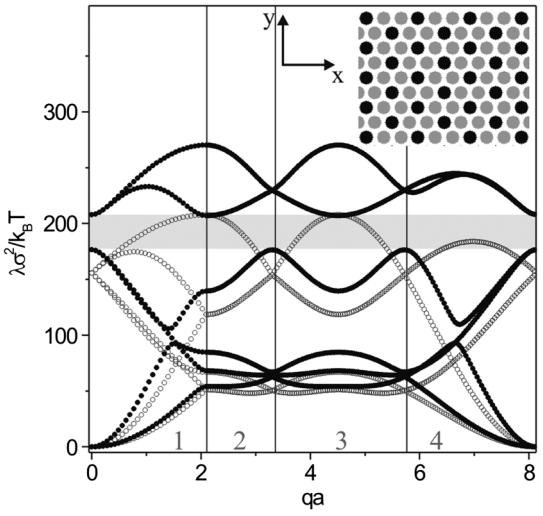

FIG. 4. Phonon band structure (solid symbols) of a paramagnetic 2D binary crystal (see inset) calculated in the harmonic approximation. The black particles in the inset have a magnetic susceptibility 20 times larger than the susceptibility of the gray particles. The magnetic field $\vec{B}$ is perpendicular to the system plane. The band gap can be closed for $\vec{B} = \vec{0}$ and $\lambda > 0$ if all the particles additionally interact via a Lennard-Jones potential (open symbols).

tems where $\lambda(\vec{q}) \to 0$ for $\vec{q} \to \vec{0}$. To overcome this limitation, one can create additional optical branches [$\lambda(\vec{q}) > 0$ for $\vec{q} = \vec{0}$]. This is achieved by extending the unit cell of the crystal by adding particles with different magnetic properties to the system (black and gray spheres in the inset of Fig. 4). For our calculations we assumed a magnetic susceptibility ratio $\chi_1/\chi_2 = 20$ between the black and gray particles and the magnetic field $\vec{B}$ orientated perpendicular to the system. The calculated phonon band structure is shown in Fig. 4 as closed symbols and indeed shows four additional optical branches. Most importantly, we observe a full band gap whose frequency $\omega \propto \sqrt{\lambda}$ and width scale linearly with the magnetic field. As a consequence, the band gap can only be closed in the limit $\vec{B} \to \vec{0}$ where both the pair interaction and the corresponding spring constants $\lambda(\vec{q})$ vanish; therefore, we considered an additional pair interaction which was exemplarily assumed as a Lennard-Jones potential $\phi_{\mathrm{LJ}}(r) \propto [(\sigma/r)^{12} - 2(\sigma/r)^6]$. Similar as above the band gap can be completely closed at $\vec{B} = \vec{0}$ but now at finite frequencies, here determined by the Lennard-Jones interaction (see open symbols in Fig. 4). This would allow to extend the possibility to tailor phononic band structure also to situations where surface potentials can not be modified. Preliminary calculations indicate that a similar behavior can be observed in three-dimensional systems.

In conclusion, we have experimentally demonstrated that the phonon band structure of a 2D colloidal crystal can be greatly tuned by the strength of periodic substrate potentials. Depending on the symmetry of the applied substrate potential different phonon polarizations can be tailored rather independently. Calculations with binary crystals of paramagnetic particles with adjustable pair interactions indicate that phononic band engineering can be also performed in situations where substrate potentials can not be tuned and thus opens novel perspectives for the fabrication of phononic crystals with band gaps adjustable by external fields.

It is a great pleasure to acknowledge H. H. von Grünberg for helpful ideas and stimulating discussions.

*j.baumgartl@physik.uni-stuttgart.de

[1] J. D. Joannopoulos, P. R. de Villeneuve, and S. Fan, Nature (London) **405**, 437 (2000).
[2] K. P. Velikov, A. Moroz, and A. van Blaaderen, Appl. Phys. Lett. **80**, 49 (2002).
[3] J. O. Vasseur, P. A. Deymier, B. Chenni, B. Djafari-Rouhani, L. Dobrzynski, and D. Prevost, Phys. Rev. Lett. **86**, 3012 (2001).
[4] Z. Liu, X. Zhang, Y. Mao, Y. Y. Zhu, Z. Yang, C. T. Chan, and P. Sheng, Science **289**, 1734 (2000).
[5] T. Gorishnyy, C. K. Ullal, M. Maldovan, G. Fytas, and E. L. Thomas, Phys. Rev. Lett. **94**, 115501 (2005).
[6] E. L. Thomas, T. Gorishnyy, and M. Maldovan, Nat. Mater. **5**, 773 (2006).
[7] W. Cheng, J. Wang, U. Jonas, G. Fytas, and N. Stefanou, Nat. Mater. **5**, 830 (2006).
[8] O. Morsch and M. K. Oberthaler, Rev. Mod. Phys. **78**, 179 (2006).
[9] J. Baumgartl, J. L. Arauz-Lara, and C. Bechinger, Soft Matter **2**, 631 (2006).
[10] Q.-H. Wei, C. Bechinger, D. Rudhardt, and P. Leiderer, Phys. Rev. Lett. **81**, 2606 (1998).
[11] A. Chowdhury, B. J. Ackerson, and N. A. Clark, Phys. Rev. Lett. **55**, 833 (1985).
[12] C. Bechinger, M. Brunner, and P. Leiderer, Phys. Rev. Lett. **86**, 930 (2001).
[13] M. Brunner, C. Bechinger, W. Strepp, V. Lobaskin, and H. H. von Grünberg, Europhys. Lett. **58**, 926 (2002).
[14] H. H. von Grünberg and J. Baumgartl, Phys. Rev. E **75**, 051406 (2007).
[15] P. Keim, G. Maret, U. Herz, and H. H. von Grünberg, Phys. Rev. Lett. **92**, 215504 (2004).
[16] P. M. Chaikin and T. C. Lubensky, *Principles of Condensed Matter Physics* (Cambridge University Press, Cambridge, England, 1995), p. 223.
[17] A sliding time window ΔT was chosen and the lattice sites $\vec{R}(t)$ at time t then followed as the temporal average $\vec{R}(t) = \Delta T^{-1} \int_{t-\Delta T/2}^{t+\Delta T/2} dt' \vec{r}_i(t')$. The displacement $\vec{u}(\vec{R}, t)$ from the lattice site $\vec{R}$ is obtained straightforwardly as $\vec{u}(\vec{R}, t) = \vec{r}_i(t) - \vec{R}(t)$. We performed the evaluation for the three values $\Delta T = 25s$, $40s$, and $60s$ and do not observe a dependence of our results on ΔT for the two larger values; therefore, $\Delta T = 40s$ is sufficiently long for accurate determination of the lattice sites $\vec{R}$.
[18] N. D. Mermin, Phys. Rev. **176**, 250 (1968).